national accelerator laboratory

TM-287
1100.300

HADRON SHIELDING CALCULATIONS: EFFECTS OF VOIDS

A. Van Ginneken

March 12, 1971

I. Introduction

Several Monte Carlo (MC) computer codes exist to simulate the internuclear cascade development in massive targets (shields). One such program, frequently used at NAL, called FLUTRA, was written by J. Ranft[1] and later modified by M. Awschalom and T. Borak.[2] In this program the shield is represented by a solid block of homogeneous composition. The beam is incident at the center of the face of the shield. The main outputs are spatial distributions of the density of energy deposition and of star density inside the shield.

The extension of such codes to heterogeneous media would be very desirable for applications to certain realistic shielding problems. As a first step FLUTRA was modified to allow voids to be present in the shield.

II. Modification of FLUTRA

Briefly, the technique employed treats voids much like the shielding material except that a "nuclear interaction" (star) within the void reproduces the incident particle

Operated by Universities Research Association Inc. Under Contract with the United States Atomic Energy Commission

identically (instead of creating an appropriate number of secondaries). This is accomplished by referencing a simple subroutine (HITORM) each time an interaction takes place, to decide whether its position is inside the shield or in a void. A similar technique is employed in connection with energy deposition.

This method was implemented in FLUTRA with relatively few changes in the main text. It has the advantage of being applicable to almost any geometry by appropriately coding the subroutine HITORM.

Below, results of this new version of FLUTRA are compared with those of simple calculations (essentially as a verification of the method) as well as with some experimental data. In addition, some applications to typical shielding geometries are discussed.

III. Comparison with Analytical Results

As a check of the procedure this new version of FLUTRA was run, slightly modified so as to compute densities of stars due to second generation particles only. Specifically, a short run was made for the case where protons (momentum $\equiv p_{inc}$) interact in an infinitesimally thin target and the resulting secondaries strike a thin shield a distance z away from the target (Fig. 1). The results can be compared directly with

the following expression of the star density (ρ_s) as a function of radius (r), for this geometry:

$$\rho_s(r) = \left\{ \sum_{i=p,n,\pi} k_i \int_{p_{c.o.}}^{p_{inc.}} \left[\frac{d^3N}{d^2\Omega dp}(\theta) \right]_i dp \right\} \Big/ \lambda(r^2+z^2) \qquad (1)$$

where $\theta \equiv \tan^{-1}(r/z)$

$\lambda \equiv$ interaction length (nonelastic)

$p_{c.o.} \equiv$ cut-off momentum (below which particles do not create stars in the MC calculation)

$\left(\frac{d^3N}{d^2\Omega dp}\right)_i \equiv$ p,n,π yield according to the modified Trilling formula[3]

$k_i \equiv$ factor reproducing FLUTRA normalization based on conservation of energy and constant inelasticities (fraction of energy carried off in a collision by particles of kind i).

To allow a more accurate comparison with the MC calculation (1) was modified to take into account the finite longitudinal width ($\equiv\Delta z$) of the volume bins used in FLUTRA to compute star densities, i.e.,

$$\rho_s'(r) = \left\{ \sum_{i=p,n,\pi} k_i \int_{p_{c.o.}}^{p_{inc.}} \left[\frac{d^3N}{d^2\Omega dp}(\theta) \right]_i dp \right\} \left[1-\exp\left(-\frac{\Delta z}{\lambda\cos\theta}\right) \right] \cos^3\theta \Big/ z^2\Delta z \qquad (2)$$

The comparison is shown in Fig. 2 for $p_{inc.} = 400$ GeV/c and z = 1m; both target and shield were assumed to be iron.

For a few MC results the uncorrelated error, based on Poisson statistics, is shown. Correlations are introduced via energy conservation. They could be significant (particularly in a short MC run) and a g with other approximations involved in (2) they could account for the small apparent systematic deviations. The two calculations agree within a factor of two over a star density variation of several orders of magnitude. Therefore, the MC calculation can be assumed to be correct.

IV. Comparison with Experiments

A. Beamstop Experiment.

In a typical beamstop experiment the beam impinges normally on a series of slabs (usually steel or concrete) and particle fluxes are measured by suitable detectors embedded between the slabs. Frequently sizable gaps separate the slabs to facilitate access to the detectors. An accurate calculation must consider the presence of these gaps. The new FLUTRA was applied to the specific geometry of such an experiment performed with 29.4 GeV protons. Since the gaps were narrow relative to the slabs, the effect was predictably small. The results are discussed elsewhere.[4]

B. Side Shield Experiment

Recently Bennett, et al.[5] performed a shielding experiment at BNL using the geometry shown in Fig. 3. The 28 GeV

proton beam was incident on a small tungsten target located at 10 inches from a large steel shield placed parallel to the beam axis. Bennett, et al. measured C^{11} produced in polyethylene foils embedded in the shield. Dimensions of the shield and approximate location of the foils are also shown in Fig. 3.

To improve the comparison additional modifications to FLUTRA were made. (a) Along with the star production the program computed C^{11} production from polyethylene using experimental excitation functions.[6] Separate excitation functions for p, n and π were used. (b) The different composition of target and shield was simulated by appropriately referencing different source terms (viz., the modified Trilling formula with parameters for tungsten or iron).

The comparison is shown in Fig. 4. With the exception of the results at large axial distances and small radii the MC calculation fits the data quite well. The largest deviation occurs for the point at zero depth and axial distance of 57.5 inches where the predicted value is too high by a factor of $\sim$ 2.5. Most other points are fitted much better. There could be many reasons for such deviations but they arise most likely from errors in the source terms. The quality of the fit is comparable to fits of the original FLUTRA to beamstop data.[4]

V. Applications to Realistic Shielding

FLUTRA, with the above modifications, was applied to two realistic shielding configurations with essentially the same geometry but with enormously different dimensions. The results are compared with those of other calculations.

A. Target in an Experimental Cave

The geometry which approximates that of a typical equipment cave is that of a hollow cylinder in which the beam travels along the axis and strikes a target (Fig. 5). Specifically both the target and the surrounding shield were assumed to be of iron. Overall dimensions were 2m (radius) and 10m length; corresponding dimensions for the cavity were 1m and 6m. The target was about one nonelastic interaction length long and 0.4cm x 0.4cm in lateral extent. The incident proton momentum in this calculation was 400 GeV/c and the threshold momentum was 0.3 GeV/c ($\simeq$ 47 MeV kinetic energy). The incident protons were assumed to be uniformly distributed over a 0.3cm x 0.3cm area at the face of the target.

Fig. 6a shows the result of FLUTRA for the average star density in the radial bin (Δr = 4cm) nearest to the inner tunnel wall. The surface star density due to secondaries only (unattenuated in the target) is also shown. This was calculated along the lines of (1). While they are not

strictly comparable (since the star density is rapidly varying as a function of radius) the effect of the cascade development in the target is clearly evident.

Fig. 6b represents the star density in the shield versus radial distance for three axial regions (0-2m, 2-4m and 4-6m). It can be seen that the radial dependence is nearly the same in each region.

The star density in the backwall of the cavity as a function of axial depth is shown in Fig. 6c at several radii (2, 10, 22, 50 and 94cm). Here, in contrast to the side wall results, both the star density at the surface as well as the depth dependence of the star density are seen to vary strongly with radius.

The total number of stars produced per incident proton in this calculation is ~ 327 (i.e., 0.82 stars per GeV/c of incident proton). As expected, this is in good agreement with results of FLUTRA for a solid beamstop of iron using identical values for the incident and threshold momenta.

B. Long Decay Tunnel

The geometry of a long decay tunnel (ν production tunnel) is practically identical to that of the equipment cave. However, dimensions and composition are quite different.

Specifically, it was assumed that the tunnel was 400m long, 0.5m in radius and surrounded by soil. The target was about one nonelastic interaction length long, 0.4cm x 0.4cm laterally and composed of iron. The incident proton momentum was 400 GeV/c and the assumed threshold momentum was 0.17 GeV/c (≃ 15 MeV kinetic energy). The incident protons were assumed to be **uniformly** distributed over a 0.3cm x 0.3cm area of the face of the target.

Fig. 7a shows the resulting average star density in the radial bin (Δr = 5cm) nearest to the inner tunnel wall. Also shown is the surface density due to secondaries only, neglecting attenuation (see A, above).

In Fig. 7b the radial dependence of the star density in the shield is shown for four axial regions. Again it can be seen that this radial dependence is remarkably the same everywhere.

The total star production in the shield was calculated to be ~ 590 stars per incident proton (or ~ 1.47 stars per GeV of incident proton kinetic energy).

Since Na^{22} production in soil shields is of some environmental concern at NAL, FLUTRA was modified to compute the spatial distribution of Na^{22} atoms in the shield. The calculation employed an excitation function estimated from

experimental data.[7] Fig. 7c presents the density of Na^{22} atoms (averaged over the entire length of the tunnel) versus radius. In the entire shield there were 6.4 Na^{22} atoms produced per incident proton. This number is likely to be an underestimate since some contributions to Na^{22} formation were neglected. Low energy particles (< 15 MeV kinetic energy) are not followed in the calculation, yet they can produce Na^{22} (mainly from Mg, which has a low threshold for Na^{22} production). These neglected particles include cascade particles below 15 MeV as well as all evaporation particles. Also neglected is the contribution due to stopped π^-. Rough estimates indicate that these sources of Na^{22} should be much smaller than those included in the calculation.

C. Relation to Other Calculations

Some calculations exist which treat problems similar to those discussed above. Goebel and Ranft[8] calculated the surface star density in iron for a tunnel of the same radius as presented above (see A), for 300 GeV/c incident protons. Unfortunately, these authors give too little detail on the assumptions underlying their calculations to make a meaningful comparison. Nonetheless it appears that their result is much higher (by about an order of

magnitude) than the corresponding star density obtained here (Fig. 6a). Qualitatively there appears to be good agreement between both calculations as to the shape of the surface star density versus axial distance curve as well as the shape of the radial dependence of the star density in the wall of the enclosure.

Gabriel and Santoro[9] performed a calculation on soil activation by 500 GeV protons in a long tunnel of similar dimensions to the case presented in B, above. Their target was beryllium and it was one interaction length long. The production model employed was the extrapolation model of Gabriel, et al.[10] In this calculation the thin target approximation was employed, i.e., only secondaries were assumed to be produced in the target. Also these authors estimated Na^{22} production probabilities from the results of MC calculations rather than from experiment.

While there is order-of-magnitude agreement with the calculations presented here, the detailed results of Gabriel and Santoro[9] are quite different from the FLUTRA predictions. The total amount of Na^{22} predicted by both calculations is in good agreement.

D. Remark on the Thin Target Approximation

Frequently in shielding calculations the assumption is made that for targets of length comparable to the

nonelastic mean free path the particles emerging from the target are the primaries which did not interact plus the secondaries produced by the interacting incident particles. Higher generation particles are neglected. This "thin target approximation" is certainly convenient since the energy spectrum at any angle is immediately given by the production model. However, depending upon the application, this can be a rather drastic over-simplification especially at high energies.

Using the "straight-ahead" approximation the number of n-th generation particles per incident proton, emitted from a target of length ℓ is

$$\left(\prod_{i=1}^{n} m_i\right) (\ell/\lambda)^{n-1} \exp(-\ell/\lambda) \Big/ (n-1)! \qquad (3)$$

where $m_i \equiv$ average number of particles (belonging to generation i) produced in a nuclear collision initiated by a particle of the (i-1)th generation.

For simplicity the m_i were assumed to equal the average number of particles emitted following the interaction of a particle having a kinetic energy equal to the average kinetic energy of an (i-1)th generation particle. These m_i were calculated from the production model used in FLUTRA (i.e., Trilling formula plus energy conservation). For

each interaction an appropriate amount of nuclear excitation energy was removed. Ionization energy losses were neglected. The cut-off momentum was 0.2 GeV/c.

In Table I the results of (3) are given for 400 GeV/c incident protons on iron targets of lengths $\ell = \lambda/2$ and $\ell = \lambda$. The m_i as well as the average kinetic energy for each generation are also shown.

Table I shows, for both examples, that the secondary production is only a small fraction of the total. In the thin target approximation the number of secondaries emitted using the same multiplicities is 7.8 for the case $\ell = \lambda$ (or ~ 0.15 of the total) and 4.9 for $\ell = \lambda/2$ (~ 0.32 of the total). In addition the predicted energy spectrum will be quite unrealistic.

The numbers in Table I are merely meant to illustrate the inadequacy of the thin target approximation in general. In fact in certain applications such as estimating gross star production or gross radionuclide production, it will clearly be quite adequate. On the other hand, in calculating, e.g., surface densities in an enclosure, it can be expected to produce serious underestimates.

E. Change of Scale

As is well known, the results for the tunnel geometry presented here can be applied to cases with different

dimensions of the cylindrical cavity.

(a) The star density at the surface of the wall of a tunnel of radius r can be written as

$$F_s(r,z) = w(\theta)\sin^2\theta/\lambda r^2 \qquad (4)$$

where $w(\theta)$ is the flux [(no.of hadrons)/(sterad.)(inc.proton)] emanating from the target (considered to be a point source) at polar angle $\theta[\equiv\tan^{-1}(r/z)]$. The surface star density corresponding to a cylindrical cavity with radius r' can then be obtained from (4):

$$F_s(r',z') = F_s(r,z)(r/r')^2 \qquad (5)$$

with $z' = r'z/r$. If F_s is nearly independent of z over a certain region (see Figs. 6a and 7a), the transformation becomes particularly simple

$$F_s(r') = F_s(r)(r/r')^2 \qquad (6)$$

(b) Moreover, if also the radial dependence of the star density is nearly independent of z (Figs. 6b and 7b), the scaling procedure can be extended to points inside the shield. If this radial dependence is represented by $F(r_1,r'')$, with $r'' \equiv$ radial distance from the surface, for a cylindrical cavity of radius r_1, then from (6), the radial dependence for a cavity of radius r_2 would be

$$F(r_2,r'') = F(r_1,r'')(r_1/r_2)^2 \qquad (7)$$

Similarly, scaling rules can be applied to obtain the surface star density in the back wall. However, since the star density at the surface as well as its radial dependence vary strongly with radius, the scaling is not readily applicable to locations inside the shield.

Frequently, when detailed experimental data or calculations are lacking, certain rules-of-thumb are substituted in shielding design. Often, in a tunnel geometry, the radial behavior of the star density is assumed to follow an exponential or a modified exponential, e.g.,

$$F(r_0,r) = k[\exp(-r/\ell)/(r+r_0)] \qquad (8)$$

where k,ℓ are constants and r_0 is the tunnel radius. Such functions can be fitted moderately well to the results in the region explored here.

Unfortunately, FLUTRA does not adequately explore the cascade (in a reasonable amount of time) at radii where (8) diverges significantly from the pure exponential fall-off. A different program of J. Ranft[11], TRANSK, introduces "particle splitting" to enhance the statistics in these regions. However, this program fails in certain fundamental ways, e.g., conservation of energy, and cannot be considered reliable. Efforts to remedy the difficulties with TRANSK as well as to explore other techniques to

achieve good statistics of star density and energy deposition at large radii are presently under way.

ACKNOWLEDGMENT

My thanks to M. Awschalom for suggestions and discussions. T. Borak collaborated on the experiment and calculations mentioned in Sec. IV-A which were presented in detail elsewhere. A. Nelson provided much appreciated help with the programming.

REFERENCES

1. J. Ranft, RHEL-RPP/N-20; J. Ranft, private communication to T. Borak.
2. M. Awschalom and T. Borak, private communication.
3. J. Ranft and T. Borak, NAL-FN-193 (1969).
4. A. Van Ginneken and T. Borak, paper presented at the 1971 Particle Accelerator Conference, Chicago, 1971.
5. G. Bennett, et al., paper presented at the 1971 Particle Accelerator Conference, Chicago, 1971; G. Bennett and T. Toohig, private communication.
6. St. Charalambus, et al., CERN/DI/HP-90 (1966) and references given therein.
7. A. Van Ginneken, NAL-TM-283 (1971).
8. K. Goebel and J. Ranft, CERN-HP-70-91 (1970).
9. T. A. Gabriel and R. T. Santoro, ORNL-TM-3262 (1970).
10. T. A. Gabriel, et al., ORNL-4542 (1970).
11. J. Ranft, CERN-MPS/Int.MU/EP-67-6 (1967).

FIGURE CAPTIONS

Fig. 1 Target and shield configuration employed to check MC versus analytical results.

Fig. 2 Comparison of MC with analytical results for the configuration of Fig. 1. Star densities are for stars due to secondaries only.

Fig. 3 Configuration, dimensions and approximate foil locations in the side shield experiment of Bennett, et al.

Fig. 4 Comparison of the experimental results of Bennett, et al. with MC calculations.

Fig. 5 Target and shield configuration for an idealized experimental equipment cave.

Fig. 6 Results for the configuration of Fig. 5 with an iron target (0.4 x 0.4 x 16.8cm long) and a cylindrical cavity with iron walls (1m radius and 6m long).

a. Star density in a cylindrical shell (Δr=4cm) adjacent to the tunnel wall, as calculated by the modified version of FLUTRA. Also shown is the result for the surface density of an analytical calculation using the "thin target" approximation.

b. Radial dependence of the star density for three axial regions (0-2m, 2-4m, 4-6m).

c. Star density versus axial depth in the back wall of the shield for selected radial distances.

Fig. 7 Results for the configuration of Fig. 5 with an iron target (0.4 x 0.4 x 16.8cm long) and a cylindrical cavity (0.5m radius, 400m long) surrounded by soil.

a. Star density in a cylindrical shell (Δr=5cm) adjacent to the tunnel wall, as calculated by the modified version of FLUTRA. Also shown is the result for the surface density of an analytical calculation using the "thin target" approximation.

b. Radial dependence of the star density for four axial regions (0-100m, 100-200m, 200-300m, 300-400m).

c. Density of Na^{22} atoms (averaged over the entire length of the tunnel) versus radial distance in the shield.

Table I

Number of particles emitted from a thick target ($\ell = \lambda$ and $\ell = \lambda/2$) using the "straight-ahead" approximation.

Generation Number	Average Kinetic Energy, GeV	Average Multiplicity, m_i	Number of Particles Emitted	
			$\ell = \lambda/2$	$\ell = \lambda$
1	400	1	0.61	0.37
2	32.3	12.4	3.76	4.56
3	5.16	6.3	5.92	14.37
4	1.19	3.8	3.75	18.20
5	0.34	2.6	1.22	11.83
6	0.11	1.6	0.20	3.79
7	0	0	0	0
Total number of particles			15.46	53.11

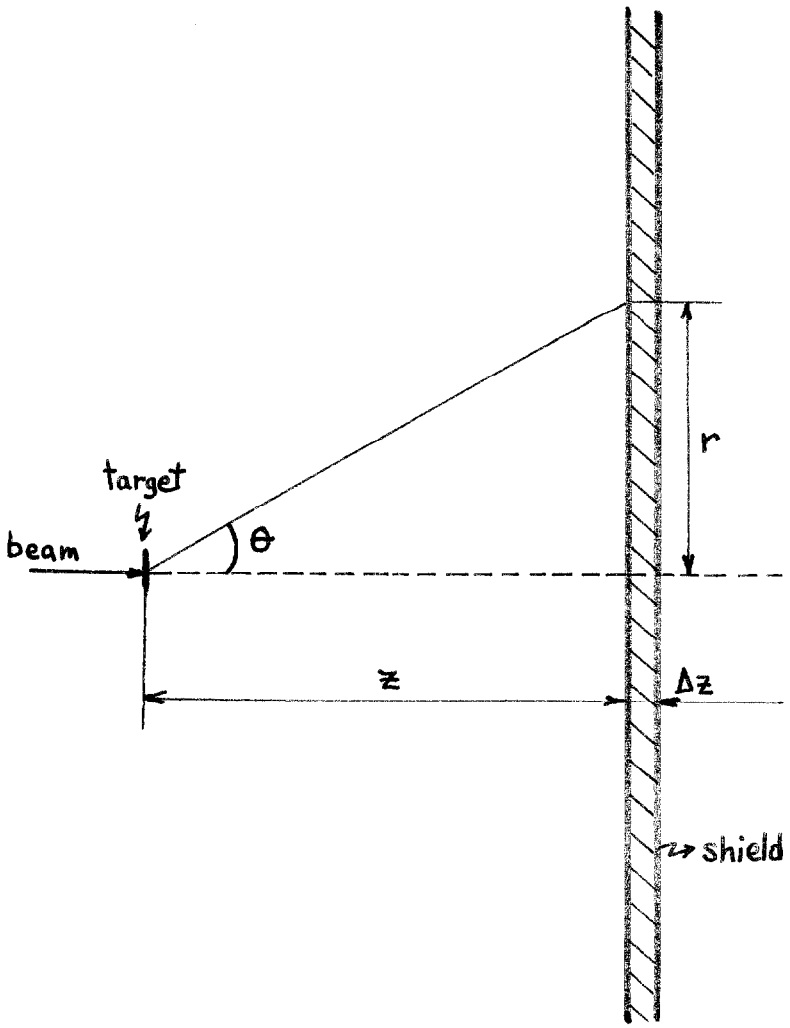

Fig. 1

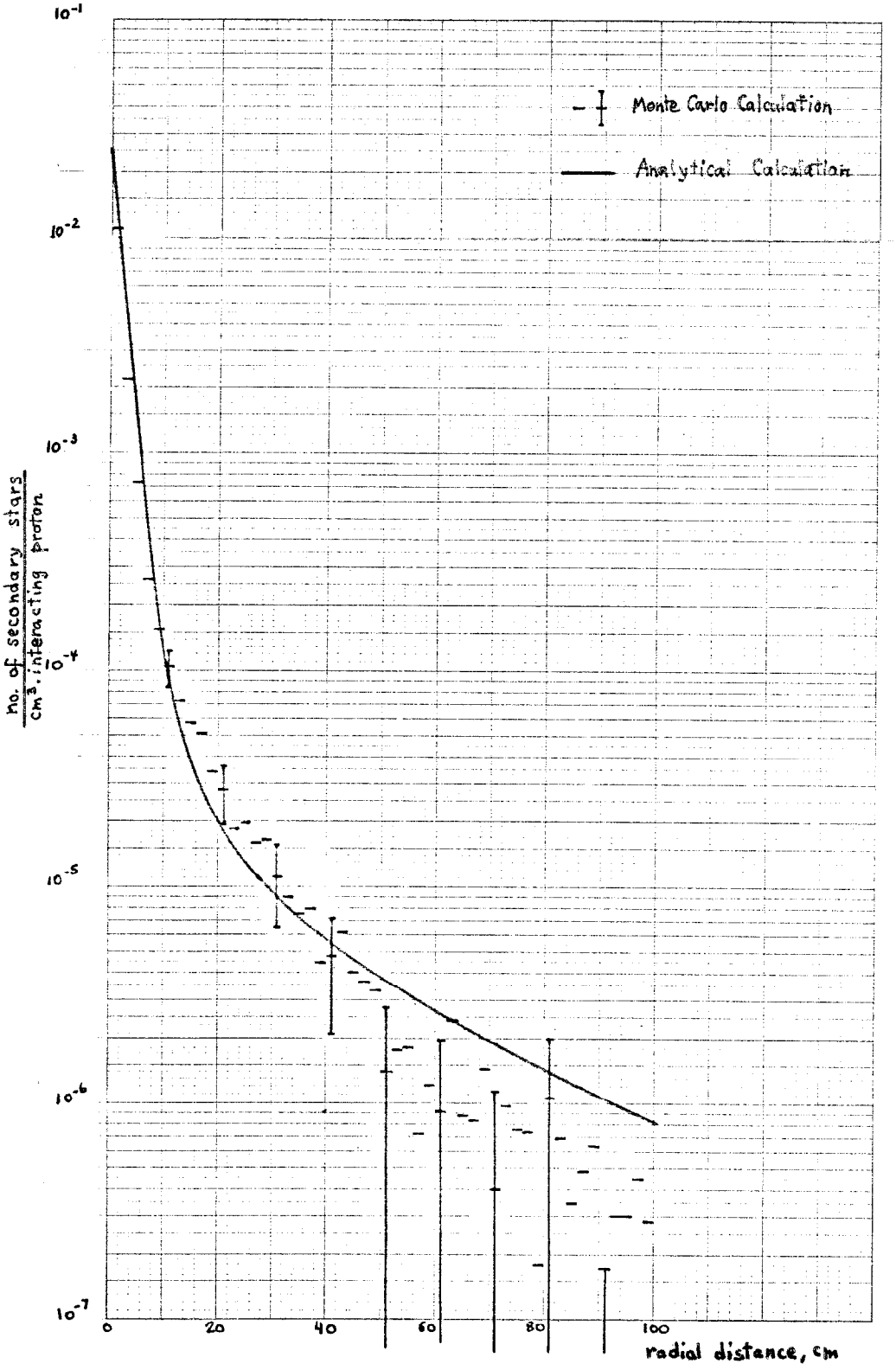
Monte Carlo Calculation
Analytical Calculation
no. of secondary stars / cm³. interacting proton
10⁻¹
10⁻²
10⁻³
10⁻⁴
10⁻⁵
10⁻⁶
10⁻⁷
0
20
40
60
80
100
radial distance, cm

Fig. 2

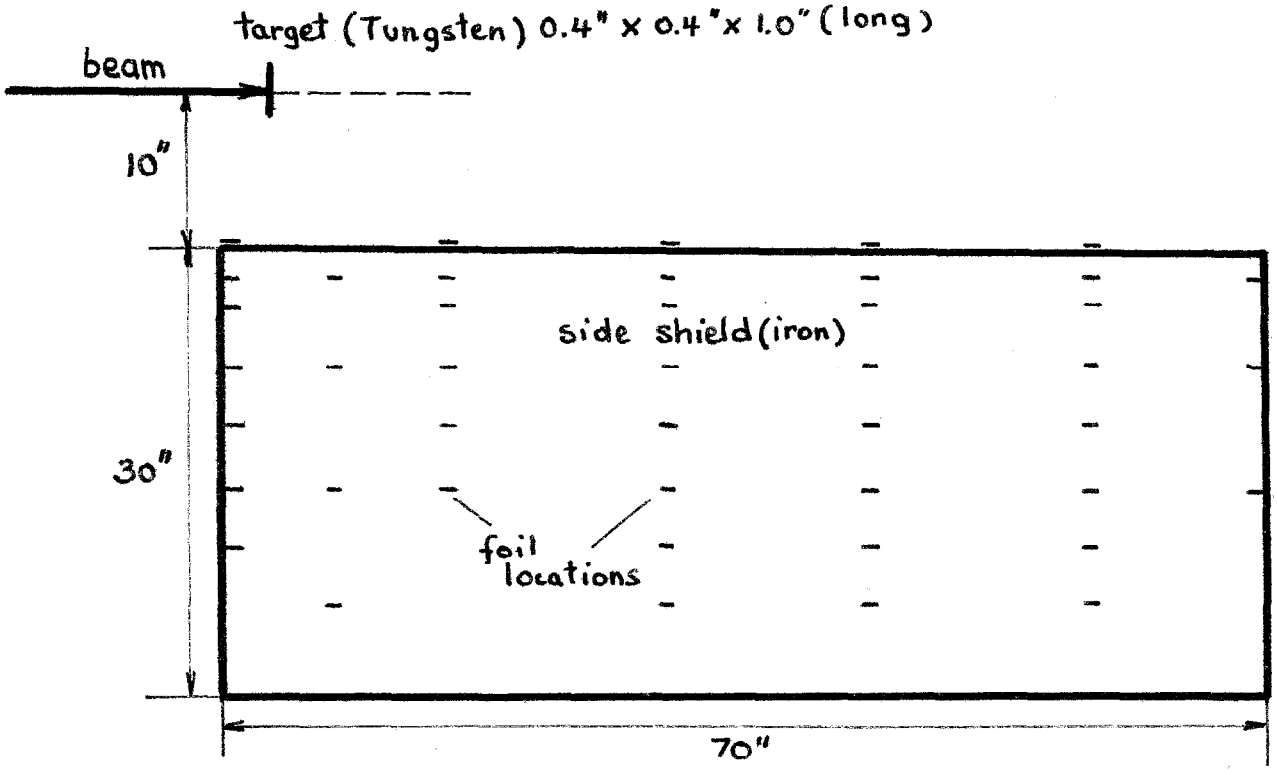
target (Tungsten) 0.4" x 0.4" x 1.0" (long)
beam
10"
side shield (iron)
30"
foil locations
70"

Fig. 3

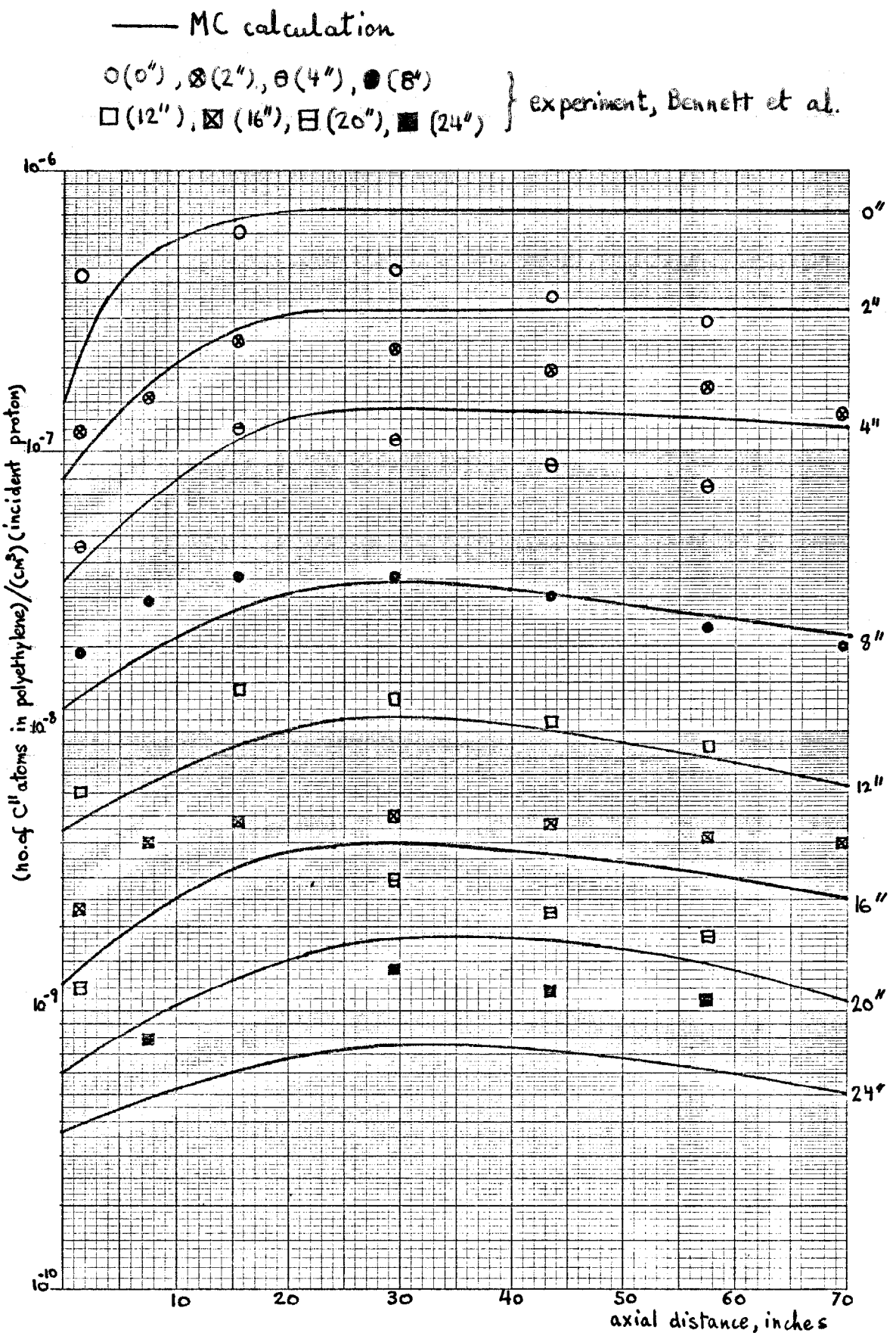
—— MC calculation
○(0″), ⊗(2″), ⊖(4″), ●(8″)
□(12″), ⊠(16″), ⊟(20″), ■(24″)
} experiment, Bennett et al.
(no. of C¹¹ atoms in polyethylene)/(cm³) (incident proton)
10⁻⁶
10⁻⁷
10⁻⁸
10⁻⁹
10⁻¹⁰
0″
2″
4″
8″
12″
16″
20″
24″
10
20
30
40
50
60
70
axial distance, inches

Fig. 4

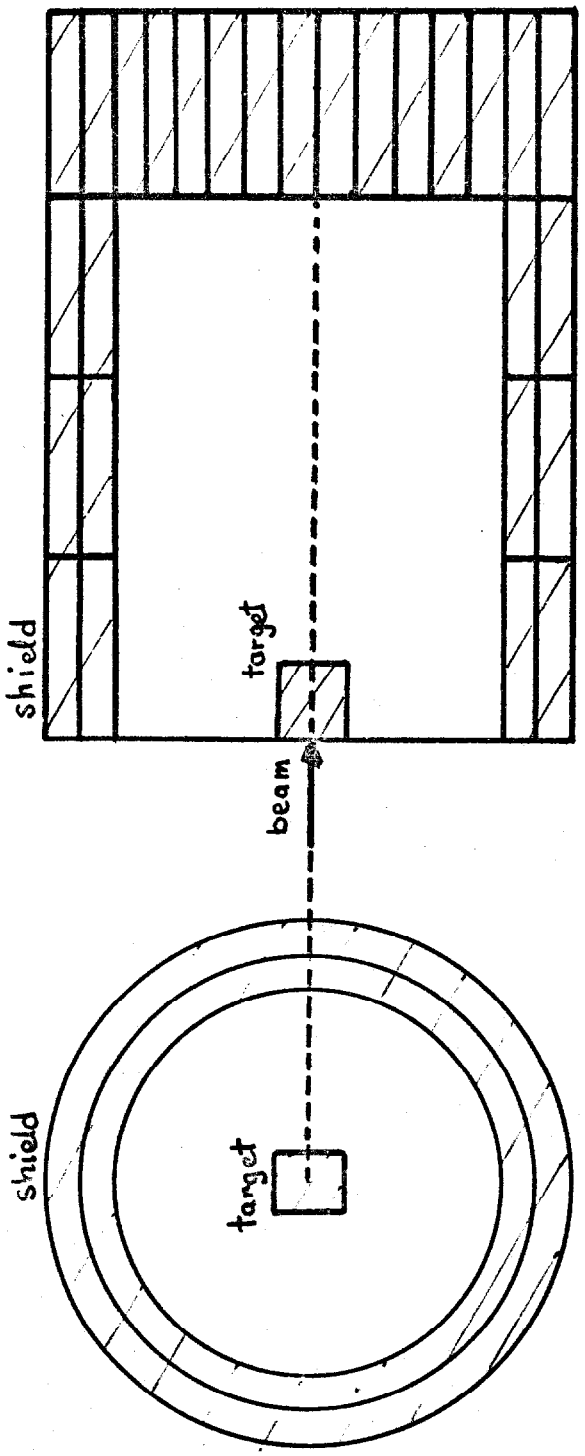

Fig. 5

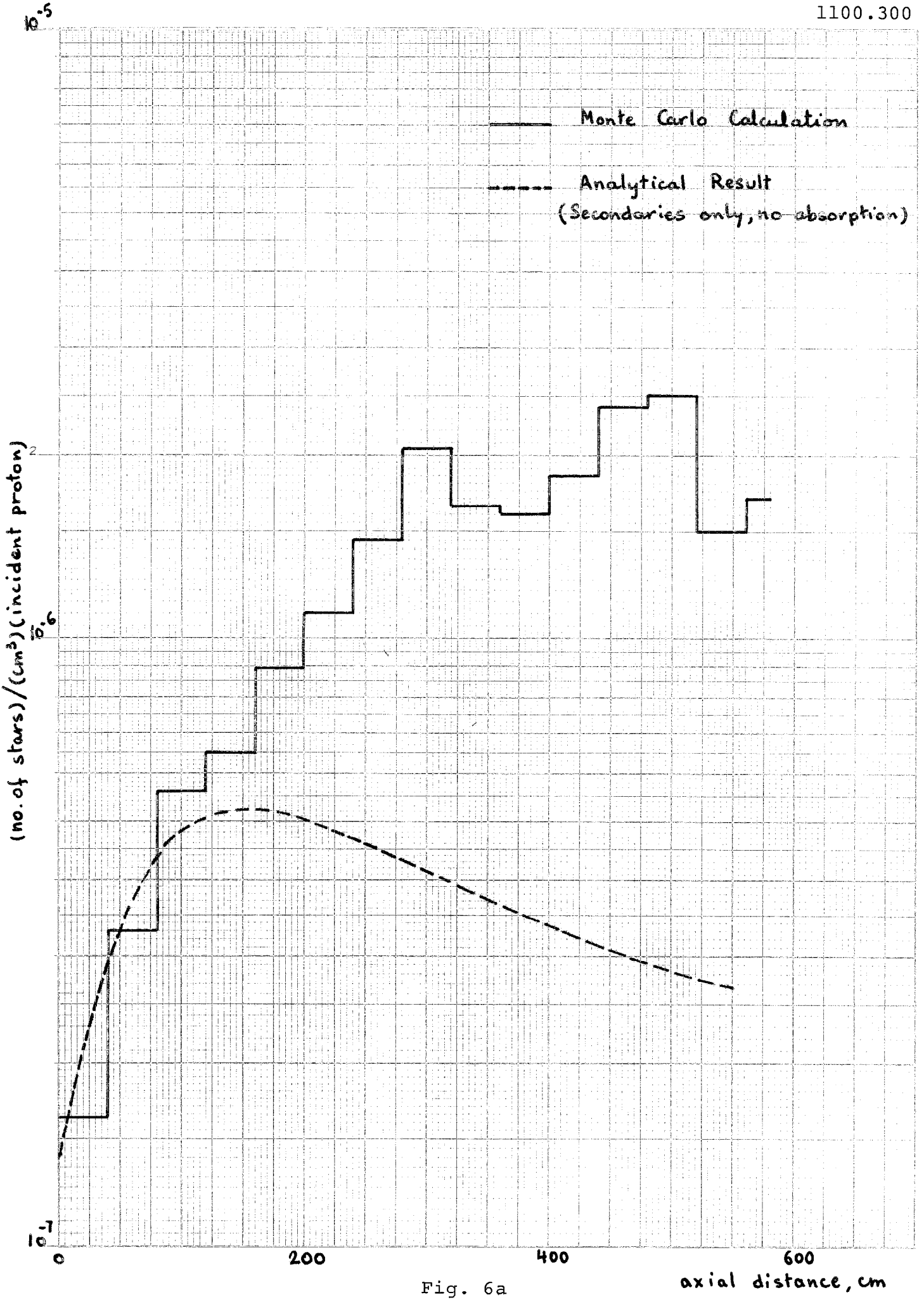
Monte Carlo Calculation
Analytical Result
(Secondaries only, no absorption)
(no. of stars)/(cm³)(incident proton)
10⁻⁵
2
10⁻⁶
10⁻⁷
0
200
400
600
axial distance, cm

Fig. 6a

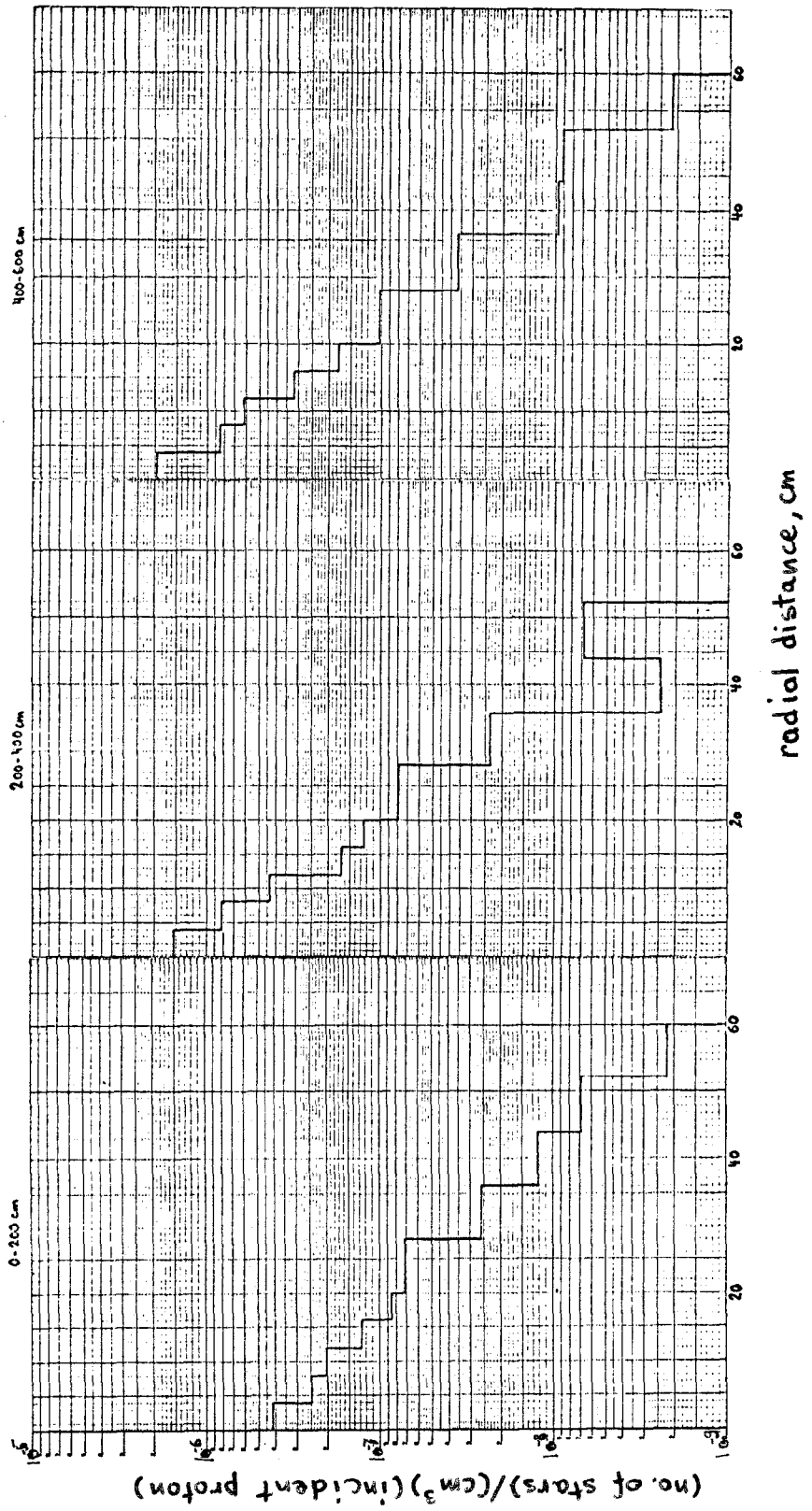
0-200 cm
200-400 cm
400-600 cm
20
40
60
radial distance, cm
(no. of stars)/(cm³)(incident proton)

Fig. 6b

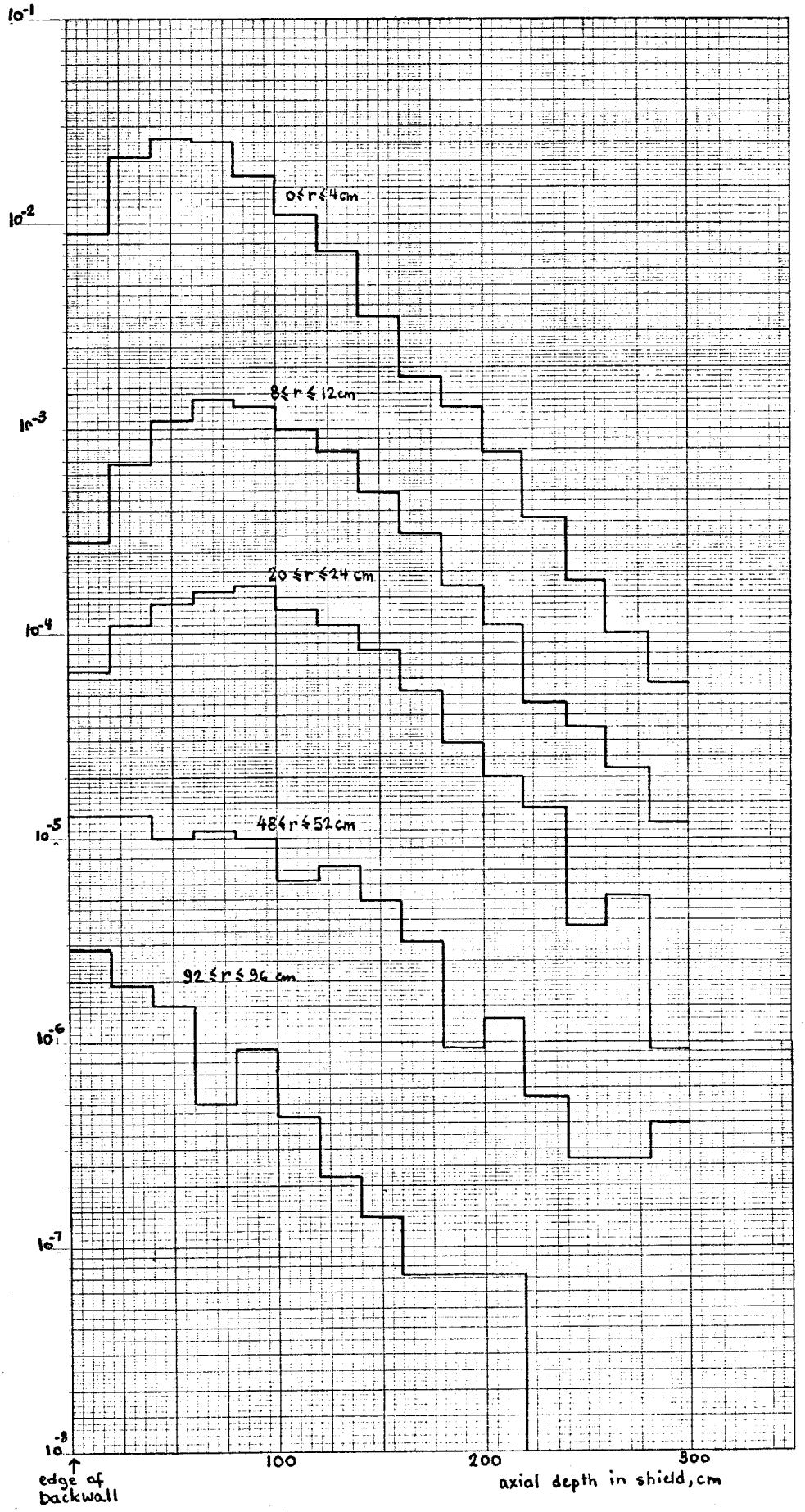
10^{-1}
10^{-2}
10^{-3}
10^{-4}
10^{-5}
10^{-6}
10^{-7}
10^{-8}
0 ≤ r ≤ 4 cm
8 ≤ r ≤ 12 cm
20 ≤ r ≤ 24 cm
48 ≤ r ≤ 52 cm
92 ≤ r ≤ 96 cm
100
200
300
edge of backwall
axial depth in shield, cm

Fig. 6c

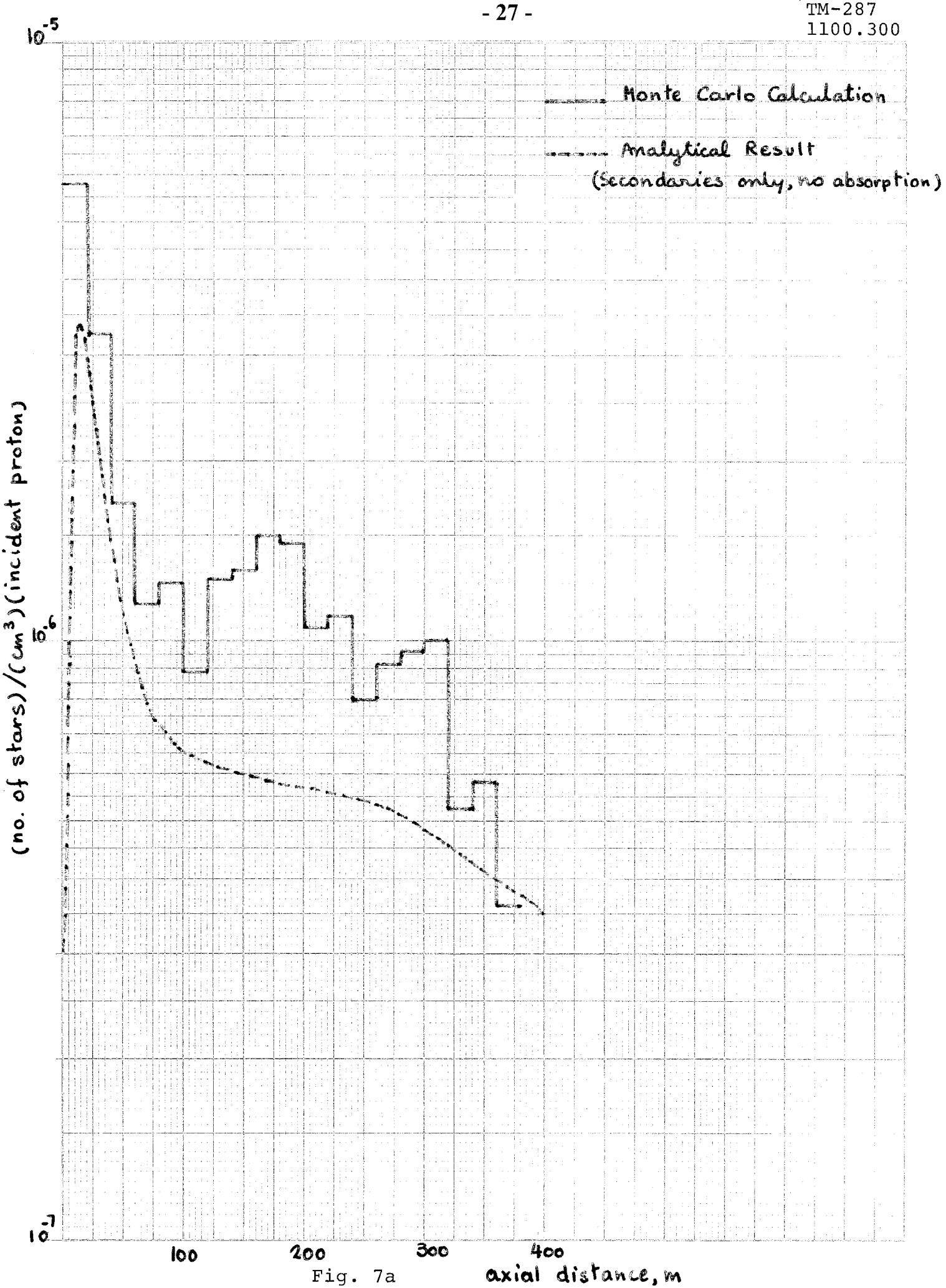
Monte Carlo Calculation
Analytical Result
(Secondaries only, no absorption)
(no. of stars)/(cm³)(incident proton)
10⁻⁵
10⁻⁶
10⁻⁷
100
200
300
400
axial distance, m

Fig. 7a

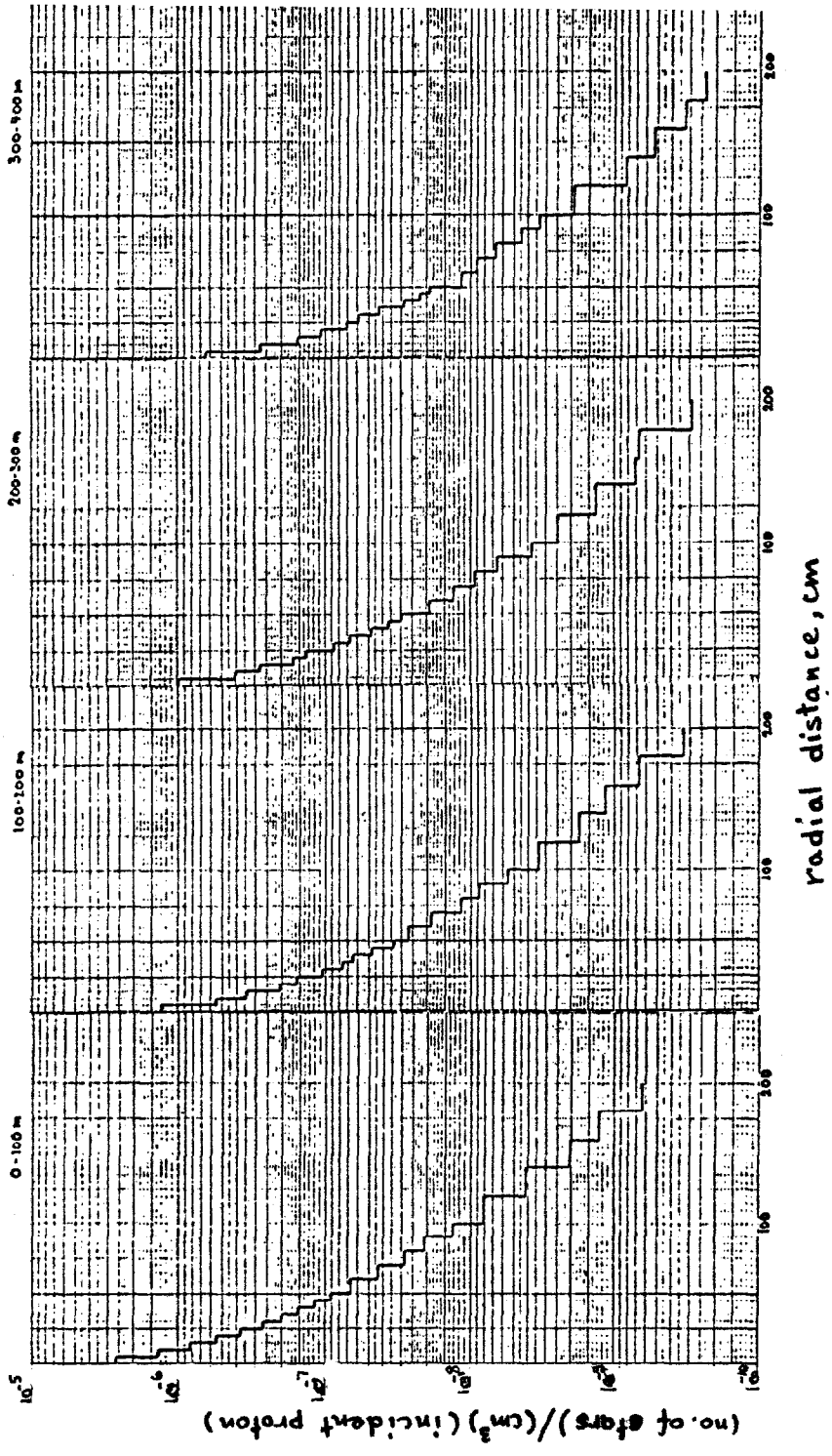
0-100 m
100-200 m
200-300 m
300-400 m
radial distance, cm
(no. of stars)/(cm³)(incident proton)

Fig. 7b

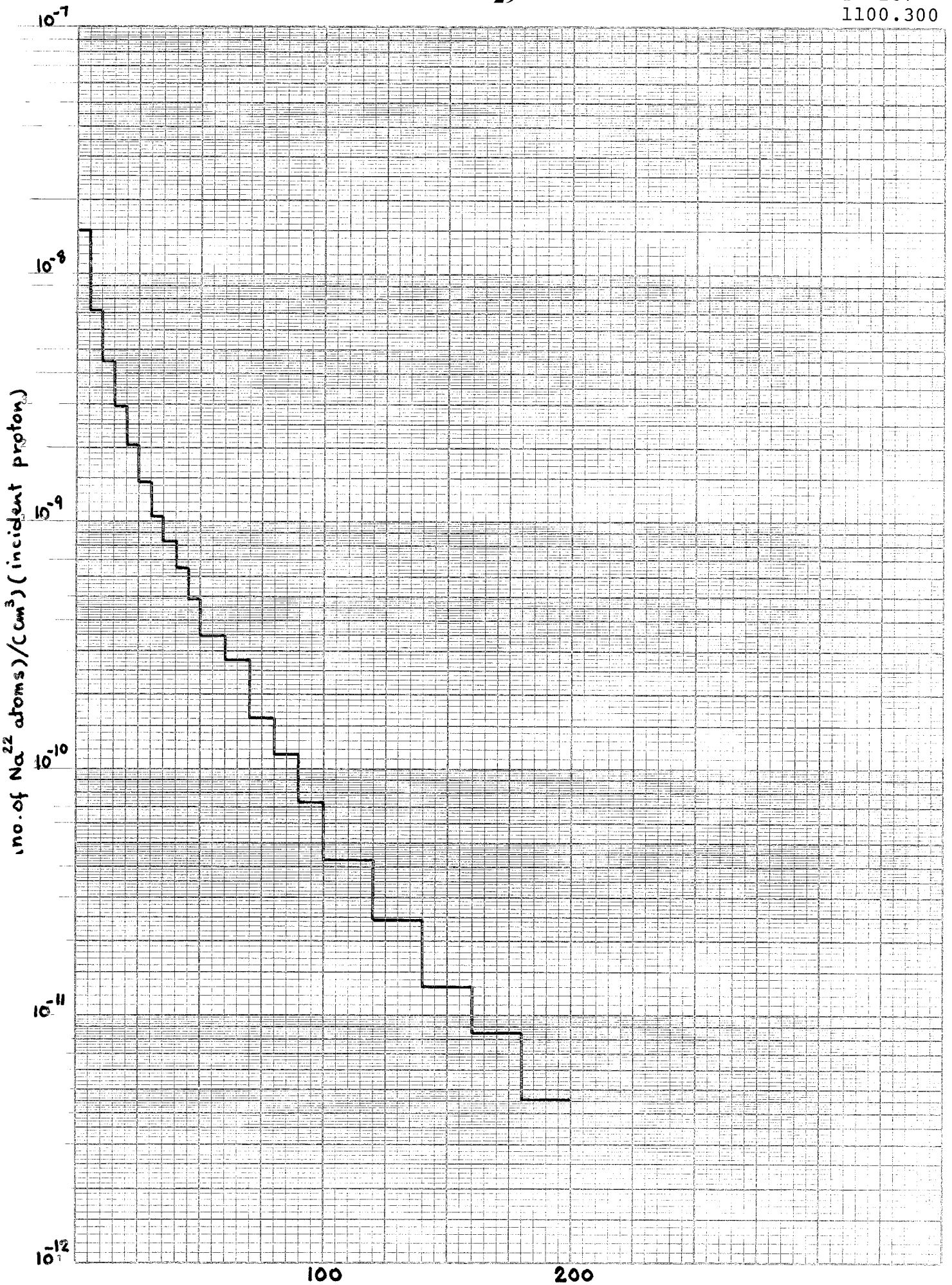
10^{-7}
10^{-8}
10^{-9}
10^{-10}
10^{-11}
10^{-12}
(no. of Na^{22} atoms)/(cm^3) (incident proton)
100
200
radial distance, cm

Fig. 7c